

Structural shape optimization of 3D nearly-incompressible hyperelasticity problems

Cláudio A.C. Silva^a and Marco L. Bittencourt^{b,*}

^aThorus Scisoft Tecnologia da Informação Ltda, Campinas, SP – Brazil

^bDepartment of Mechanical Design (DPM), Faculty of Mechanical Engineering (FEM), State University of Campinas (UNICAMP), Campinas, SP – Brazil

Abstract

This paper presents shape optimization of nearly incompressible hyperelastic structural problems. Initially, the Mooney-Rivlin hyperelastic model is reviewed. The finite element solution using a perturbed Lagrangian description and the Newton-Raphson method are discussed. The projected pressure method is used to solve the mixed problem using a standard one-field finite element procedure. The expressions of shape sensitivity are presented. Finally, the shape optimization of an engine mount geometry is considered using 2D and 3D finite element models.

Keywords: shape optimization, hyperelasticity, Finite Element Method, sensitivity analysis

1 Introduction

The formulation of the non linear hyperelasticity problem has been still studied due to the need of more precise material constitutive equations, the application of the incompressibility constraint and numerical stability. Alternative finite element techniques were developed [5, 6, 8] to the classical mixed formulation [33]; meshfree solution methods have also been used [5, 9].

The incompressible or nearly-incompressible hyperelasticity, including geometric non linearities, has been the basis of the elastic formulation of finite elastoplasticity [29]. Consequently, it is important in the analysis of practical problems of impact and fabrication processes based on plastic deformation such as forging, lamination and stamping.

In [15], a meshfree based code was applied to the sensitivity analysis and optimization of elastometer components, modeled with nearly-incompressible non linear hyperelasticity. Later, [24] extended this work including contact with friction. The advantage of the response analysis method applied in these works is the attainment of the same precision with a smaller number of degrees freedom when compared to low order h finite elements for situations of severe deformation of the domain. In shape optimization applications, the advantage of meshfree methods is the trivial process needed to mesh update since there is not interpolation distortion. The process

*Corresp. author email: mlb@fem.unicamp.br

Received 21 Aug 2007; In revised form 30 Apr 2008

consists only in replacing the functional support without changing its geometry. The disadvantage is the more complex procedure to obtain the discrete form of the sensitivity equations. The finite element method still continues to be applied to reversible problems [10].

The application of shape optimization and the finite element method in hyperelasticity was presented in [12, 17]. Instead of treating the solution of the equilibrium equation as a sub problem of the optimization cycle, this equation is modeled as an equality restriction of the optimization problem. Based on that, the non linear equilibrium and optimization problems are solved simultaneously. This represents a significative reduction in the total time needed to reach the optimum design. However, this strategy does not allow the mesh updating without interrupting the optimization process, even if there is distortion during the sequence of geometry changes. There is also little flexibility in the application of external actions (i.e. loads applied in different load steps) and equilibrium problems that are dependent on the load history are not considered.

In [21], from the response and sensitivity analysis formulations for non linear geometric and hyperelasticity, a meshfree method was used. Frictionless contact, infinitesimal plasticity and transient dynamics already used with the finite element method were incorporated. Extensions to finite plasticity and frictionless contact were also considered and applied to optimization of stamping processes [23]. One of the main interests in the research on optimization and sensitivity of non linear structural problems have been the application of systematic design methods to fabrication processes in plastic deformation [1, 2, 13, 14, 25, 34] and plastic injection [30–32].

Other approaches have been used to avoid mesh regeneration during the optimization process [19, 20, 22]. The main idea is to embed the design domain in a larger fixed fictitious domain. An Eulerian formulation may be also used as well adaptive procedures based on wavelets. However, the examples considered in the references are for 2D domains.

This work considers the shape optimization of nearly incompressible hyperelasticity and large deformation problems based on the finite element method. In [5, 9], meshfree methods were used. Initially, a review of the hyperelasticity model and the finite element solution with the Newton-Raphson procedure is considered. The equations for shape sensitivity analysis are then deduced. Finally, the procedures are applied to the shape optimization of an internal combustion engine cushion. The geometry is modeled with NURBS and the procedures for velocity fields, geometry updating and mesh distortion control discussed in [27, 28] are used. The main contribution of the paper is the combination of finite element analysis, shape sensitivity analysis, minimization procedure, mesh distortion control, NURBS and geometry updating to the shape optimization of 3D hyperelastic problems.

2 Hyperelasticity model

In this section, the symbols Lin^+ , Orth^+ and Psym are used to denote, respectively, the sets of tensors with positive determinant, rotations and symmetric positive definite tensors.

Consider the constitutive equation of a Cauchy elastic material $\mathbf{T} = \boldsymbol{\Upsilon}(\mathbf{F})$ based on the first Piola-Kirchhoff tensor \mathbf{T} [26]. The strain power density is $\mathbf{T} \cdot \dot{\mathbf{F}} = \boldsymbol{\Upsilon}(\mathbf{F}) \cdot \dot{\mathbf{F}}$. Consider a scalar function $W(\mathbf{F})$ such that

$$\dot{W}(\mathbf{F}) = DW(\mathbf{F}, \mathbf{X})[\dot{\mathbf{F}}] = \frac{\partial W}{\partial \mathbf{F}}(\mathbf{F}) \cdot \dot{\mathbf{F}} = \boldsymbol{\Upsilon}(\mathbf{F}) \cdot \dot{\mathbf{F}}. \quad (1)$$

In this case, the first Piola-Kirchhoff stress tensor is the derivative of $W(\mathbf{F}, \mathbf{X})$ with respect to \mathbf{F} with \mathbf{X} fixed, that is,

$$\mathbf{T} = \boldsymbol{\Upsilon}(\mathbf{F}, \mathbf{X}) = DW(\mathbf{F}, \mathbf{X}) = \frac{\partial W}{\partial \mathbf{F}}(\mathbf{F}, \mathbf{X}). \quad (2)$$

The previous relation is valid for a material without internal restrictions in which the components of $\dot{\mathbf{F}}$ are independent. The functional $W(\mathbf{F})$ is called strain energy density.

For objective isotropic elastic materials then $W(\mathbf{F}\mathbf{Q}) = W(\mathbf{F})$ or $W(\mathbf{Q}\mathbf{F}) = W(\mathbf{F})$ for $\mathbf{Q} \in \text{Orth}^+$. $W(\mathbf{F})$ can be determined by its restriction to Psym , that is, $W(\mathbf{F}) = W(\mathbf{R}\mathbf{U}) = W(\mathbf{U})$ or $W(\mathbf{F}) = W(\mathbf{V}\mathbf{R}) = W(\mathbf{V})$, where $\mathbf{U}, \mathbf{V} \in \text{Psym}$ are obtained from the polar decomposition of \mathbf{F} . Therefore, W can also be written as a function of \mathbf{C} or \mathbf{B} .

Combining isotropy and objectivity, it is possible to show that $W(\mathbf{Q}\mathbf{U}\mathbf{Q}^T) = W(\mathbf{U})$. W is therefore an isotropic scalar function of \mathbf{U} [26]. It is also a function of the invariants $\iota_1(\mathbf{U}), \iota_2(\mathbf{U}), \iota_3(\mathbf{U})$ or equivalently a symmetric function of the eigenvalues $\lambda_1, \lambda_2, \lambda_3$ of \mathbf{U} , in such a way that $W(\mathbf{U}) \equiv W(\mathbf{V}) = W(\lambda_1, \lambda_2, \lambda_3) = W(\lambda_1, \lambda_3, \lambda_2) = W(\lambda_3, \lambda_1, \lambda_2)$.

According to Rivlin, the strain energy function can be written in terms of an infinite power series of the three invariants I_1, I_2, I_3 of the right Cauchy-Green deformation tensor $\mathbf{C} = \mathbf{U}^2 = \mathbf{F}^T\mathbf{F}$. It is assumed that W is continuously differentiable with respect to I_1, I_2, I_3 and can be written as an infinite power series of $(I_1 - 3), (I_2 - 3)$ and $(I_3 - 1)$ as [26]

$$W(\mathbf{C}) = \sum_{i,j,k=0}^{\infty} A_{ijk} (I_1 - 3)^i (I_2 - 3)^j (I_3 - 1)^k. \quad (3)$$

Expressions usually applied are obtained for $A_{ijk} = 0$ ($k = 1, 2, 3, \dots / i, j \neq 0$)

$$W(I_1, I_2, I_3) = \sum_{i,j=0}^{\infty} A_{ij0} (I_1 - 3)^i (I_2 - 3)^j + \sum_{r=1}^{\infty} A_{00r} (I_3 - 1)^r \quad (4)$$

or $A_{ijk} = 0$ ($j, k = 1, 2, 3, \dots / i, j \neq 0$)

$$W(I_1, I_2, I_3) = \sum_{i,j=0}^{\infty} A_{i00} (I_1 - 3)^i + \sum_{r=1}^{\infty} A_{00r} (I_3 - 1)^r. \quad (5)$$

For incompressible materials, $I_3 = \det \mathbf{F} = J = 1$ and W is dependent only of the other two invariants. In this case, the Rivlin series (3) reduces to

$$\bar{W}(I_1, I_2) = \sum_{i,j=0}^{\infty} A_{ij} (I_1 - 3)^i (I_2 - 3)^j. \quad (6)$$

The Rivlin infinite series is usually truncated in the Mooney-Rivlin or neo-Hookean forms given, respectively, as [26]

$$\bar{W}(I_1, I_2) = A_{10} (I_1 - 3) + A_{01} (I_2 - 3), \quad (7)$$

$$\bar{W}(I_1, I_2) = A_{10} (I_1 - 3). \quad (8)$$

The material constants in (7) and (8) obtained from experiments are generally appropriated only for moderated finite deformations. They may not reproduce precisely experimental data for very large deformation [6]. Reasonable results have been obtained in the numerical simulation of rubber using the cubic and the modified cubic functions given, respectively, by [8, 9]

$$\bar{W}(I_1, I_2) = A_{10} (I_1 - 3) + A_{20} (I_1 - 3)^2 + A_{30} (I_1 - 3)^3, \quad (9)$$

$$\bar{W}(I_1, I_2) = \frac{\alpha}{\beta} \left[1 - e^{-\beta(I_1-3)} \right] + A_{10} (I_1 - 3) + A_{20} (I_1 - 3)^2 + A_{30} (I_1 - 3)^3. \quad (10)$$

On the other hand, (7) and (8) allow to study satisfactorily the behavior of hyperelastic materials for the development of numerical algorithms [21, 24].

For isotropic material, the strain energy functional can be written as $W \equiv W(\mathbf{C})$. Therefore,

$$\dot{W}(\mathbf{C}) = DW(\mathbf{C}, \mathbf{X})[\dot{\mathbf{C}}] = \frac{\partial W}{\partial \mathbf{C}}(\mathbf{C}) \cdot \dot{\mathbf{C}}.$$

It may be observed that

$$\dot{W}(\mathbf{F}) = \frac{\partial W}{\partial \mathbf{F}}(\mathbf{F}) \cdot \dot{\mathbf{F}} = \mathbf{T} \cdot \dot{\mathbf{F}} = \mathbf{S} \cdot \dot{\mathbf{E}} = \frac{\partial W}{\partial \mathbf{C}}(\mathbf{C}) \cdot \dot{\mathbf{C}} = \dot{W}(\mathbf{C}).$$

From there, the following total Lagrangian constitutive equation, which relates the second Piola-Kirchhoff tensor and the Green strain tensor, can be written as

$$\mathbf{S}(\mathbf{C}, \mathbf{X}) = 2 \frac{\partial W}{\partial \mathbf{C}} = \frac{\partial W}{\partial \mathbf{E}}. \quad (11)$$

The simplest form of incompressibility constraint, which is valid for $\det \mathbf{F} = 1$, is a scalar function h sufficiently regular such that

$$h(\mathbf{F}) = 0. \quad (12)$$

If h is an objective function, then $h(\mathbf{QF}) = h(\mathbf{F})$ for every $\mathbf{Q} \in \text{Orth}^+$, $\mathbf{F} \in \text{Lin}^+$. Considering the same hypotheses assumed for W , h can be written as a function of the deformation only.

In terms of the tensor \mathbf{U} , $h(\mathbf{F}) = h(\mathbf{R}\mathbf{U}) = h(\mathbf{U}) = 0$, $\mathbf{R} \in \text{Orth}^+$. For the tensor \mathbf{C} , $\tilde{h}(\mathbf{C}) = \tilde{h}(\mathbf{U}^2) = h(\mathbf{C}^{1/2}) = 0$.

The differentiation of (12) gives

$$\dot{h}(\mathbf{F}) \equiv \frac{\partial h}{\partial \mathbf{F}}(\mathbf{F}) \cdot \dot{\mathbf{F}} = 0. \quad (13)$$

From the variational principle, a multiple of $\partial h / \partial \mathbf{F}$ can be added to the constitutive equation without affecting the strain power for all deformation gradients compatible with (12). This results in the restricted constitutive equation

$$\mathbf{T} = \mathbf{\Upsilon}(\mathbf{F}) + q \frac{\partial h}{\partial \mathbf{F}}(\mathbf{F}), \quad q \in \text{Re}. \quad (14)$$

Therefore,

$$DJ[\Delta \mathbf{F}] = (\det \mathbf{F}) \text{tr}(\mathbf{F}^{-1} \Delta \mathbf{F}) = (\det \mathbf{F}) (\mathbf{F}^{-T} \cdot \Delta \mathbf{F}) \Rightarrow \frac{\partial J}{\partial \mathbf{F}} = (\det \mathbf{F}) \mathbf{F}^{-T}.$$

As $\det \mathbf{F} = 1$, then

$$\frac{\partial h}{\partial \mathbf{F}}(\mathbf{F}) = \mathbf{F}^{-T}.$$

Substituting the above expression in (14), the equations $\mathbf{T} = \mathbf{\Upsilon}(\mathbf{F}) + q \mathbf{F}^{-T}$ and $\mathbf{S} = \mathbf{F}^{-1} \mathbf{T} = \mathbf{F}^{-1} \mathbf{\Upsilon}(\mathbf{F}) + q \mathbf{C}^{-1}$ result, respectively, for the first and second Piola-Kirchhoff tensors. Using the relation $\sigma = \mathbf{T} \mathbf{F}^T (\det \mathbf{F})^{-1}$ between the Cauchy stress tensor σ and the first Piola-Kirchhoff tensor \mathbf{T} , it is possible to determine the Cauchy stress constitutive equation with incompressibility constraint

$$\sigma = \mathbf{\Sigma}(\mathbf{F}) + q \mathbf{I}, \quad \mathbf{\Sigma}(\mathbf{F}) = \mathbf{\Upsilon}(\mathbf{F}) \mathbf{F}^T. \quad (15)$$

The main invariants of the tensor $\mathbf{C}^* = \mathbf{F}^{*T} \mathbf{F}^*$ are $\bar{I}_1 = I_1 I_3^{-1/3}$, $\bar{I}_2 = I_2 I_3^{-2/3}$ and $\bar{I}_3 = 1$, where $\mathbf{F}^* = J^{-1/3} \mathbf{F}$. From these relations, the terms related to distortion and dilatation of the constitutive equation can be separated.

Consider a configuration change of a generic compressible material body expressed in terms of the isochoric displacement gradient $\mathbf{F}^* = J^{-1/3} \mathbf{F}$. In this case, the strain energy is $W^*(\mathbf{F}^*, J) \equiv W(\mathbf{F})$.

For hyperelastic materials,

$$\mathbf{T} = \frac{\partial W}{\partial \mathbf{F}} = \frac{\partial W^*}{\partial \mathbf{F}} = \frac{\partial W^*}{\partial \mathbf{F}^*} \frac{\partial \mathbf{F}^*}{\partial \mathbf{F}} + \frac{\partial W^*}{\partial J} \frac{\partial J}{\partial \mathbf{F}}. \quad (16)$$

Applying the definition of \mathbf{F}^* then

$$\begin{aligned} \frac{\partial \mathbf{F}^*}{\partial \mathbf{F}} &= \frac{\partial [J^{-1/3} \mathbf{F}]}{\partial \mathbf{F}} = \frac{\partial (J^{-1/3})}{\partial \mathbf{F}} \otimes \mathbf{F} + J^{-1/3} \left(\frac{\partial \mathbf{F}}{\partial \mathbf{F}} \right) \\ &= J^{-1/3} \left(\mathcal{I} - \frac{1}{3} \mathbf{F}^{*-T} \otimes \mathbf{F}^* \right), \end{aligned} \quad (17)$$

where \mathcal{I} is the fourth order symmetric identity tensor.

Substituting (17) in (16) then

$$\mathbf{T} = J^{-1/3} \left[\frac{\partial W^*}{\partial \mathbf{F}^*} - \frac{1}{3} \text{tr} \left(\frac{\partial W^*}{\partial \mathbf{F}^*} \mathbf{F}^{*T} \right) \mathbf{F}^{*-T} + J \frac{\partial W^*}{\partial J} \mathbf{F}^{*-T} \right].$$

Therefore, the first Piola-Kirchhoff tensor can be written as [26]

$$\mathbf{T} = \frac{\partial W}{\partial \mathbf{F}} = \frac{\partial W^*}{\partial \mathbf{F}^*} \frac{\partial \mathbf{F}^*}{\partial \mathbf{F}} = J^{-1/3} \left(\frac{\partial W^*}{\partial \mathbf{F}^*} + q^* \mathbf{F}^{*-T} \right), \quad (18)$$

where

$$q^* = -\frac{1}{3} \text{tr} \left(\frac{\partial W^*}{\partial \mathbf{F}^*} \mathbf{F}^{*T} \right) + J \frac{\partial W^*}{\partial J}. \quad (19)$$

Taking into account that $\mathbf{C} = J^{2/3} \mathbf{C}^*$, it is possible to determine analogously the respective equation for the second Piola-Kirchhoff tensor as

$$\mathbf{S} = J^{-2/3} \left[\frac{\partial W^*}{\partial \mathbf{E}^*} - \frac{1}{3} \left(\mathbf{C}^* \cdot \frac{\partial W^*}{\partial \mathbf{E}^*} \right) \mathbf{C}^{*-1} + J \frac{\partial W^*}{\partial J} \mathbf{C}^{*-1} \right].$$

As the Cauchy stress is given by $\sigma = J^{-1} \mathbf{T} \mathbf{F}^T$, then from (18)

$$\sigma = J^{-1} \left[\frac{\partial W^*}{\partial \mathbf{F}^*} \mathbf{F}^{*T} - \frac{1}{3} \text{tr} \left(\frac{\partial W^*}{\partial \mathbf{F}^*} \mathbf{F}^{*T} \right) \right] + \frac{\partial W^*}{\partial J} \mathbf{I}.$$

The part of σ related to dilatation is the mean normal stress \bar{p} . From the above expression, it assumes the form

$$\bar{p} = \frac{1}{3} \text{tr}(\sigma) = \frac{\partial W^*}{\partial J}.$$

The terms $\frac{\partial W^*}{\partial J}$ and $J^{-1} \left[\frac{\partial W^*}{\partial \mathbf{F}^*} \mathbf{F}^{*T} - \frac{1}{3} \text{tr} \left(\frac{\partial W^*}{\partial \mathbf{F}^*} \mathbf{F}^{*T} \right) \right]$ are related to dilatation and distortion, respectively.

It is possible to demonstrate that for nearly-incompressible materials, the strain energy density can be decomposed as the sum of distortional \bar{W} and volumetric \tilde{W} energies as [6]

$$W(\bar{I}_1, \bar{I}_2, I_3) = \bar{W}(\bar{I}_1, \bar{I}_2) + \tilde{W}(I_3). \quad (20)$$

For nearly-incompressible materials, the dilatation energy can be rewritten as [5]

$$\tilde{W}(I_3) = \frac{1}{\varepsilon} G(J), \quad (21)$$

where ε is a small parameter that indicates the compressibility degree. Formally, $\varepsilon \rightarrow 0$ and $G(J) \rightarrow 0$ (faster than ε) corresponds to the incompressibility condition. In this case, it is possible to eliminate $\tilde{W}(I_3)$ in (20). An example of a function $\tilde{W}(I_3)$ is ([5])

$$\tilde{W}(I_3) = \frac{1}{\varepsilon} \left[\frac{1}{2} (J^2 - 1 - 2 \ln J) \right]. \quad (22)$$

In this case, the hydrostatic pressure is

$$\bar{p} = \frac{\partial W^*}{\partial J} = \frac{\partial \tilde{W}}{\partial J} = \frac{1}{\varepsilon} \left(J - \frac{1}{J} \right).$$

For nearly-incompressible materials, J is close to 1 and

$$\bar{p} \approx \frac{1}{\varepsilon} (J - 1) = \frac{1}{\varepsilon} \left(\frac{\rho_0}{\rho} - 1 \right).$$

A usual solution found in the literature is to consider the above approximation which corresponds to the following dilatation energy density functional [3, 5–9, 15, 21]

$$\tilde{W}(I_3) = \frac{1}{2\varepsilon} (J - 1)^2 \quad (23)$$

together with (7), (8), (9) or (10) for incompressible material. Therefore, they are functions of isochoric deformation gradients \mathbf{F}^* and generate approximately incompressible forms of these material models. For example, [21]

$$W(\bar{I}_1, \bar{I}_2, J) = A_{10} (\bar{I}_1 - 3) + A_{01} (\bar{I}_2 - 3) + \frac{\tilde{\kappa}}{2} (J - 1)^2. \quad (24)$$

The term $\tilde{\kappa} = 1/\varepsilon$ is physically interpreted as the bulk modulus.

3 Numerical techniques for response analysis

3.1 Nearly-incompressible and incompressible Materials

For a nearly-incompressible isotropic hyperelastic material, the strain energy density functional is given by (20) and (21). It is demonstrated that the solution of the hyperelastic problem, expressed in a standard variational form, exists if \bar{W} and G follow certain hypotheses [5]. Consider the limit behavior of the variational principle for $\varepsilon \rightarrow 0^+$, that is,

$$\Pi^\varepsilon(\mathbf{x}^\varepsilon) = \inf_{\chi \in \mathcal{V}} \Pi^\varepsilon(\chi), \quad (25)$$

where \mathcal{V} is a suitable Hilbert functional space in such a way that $\det \mathbf{F} > 0$ and

$$\Pi^\varepsilon(\chi) = \int_{\mathcal{B}} \left[\bar{W}(\bar{I}_1(\chi), \bar{I}_2(\chi)) + \frac{1}{\varepsilon} G(J(\chi)) \right] dV - W_{ext}(\mathbf{X}, \chi(\mathbf{X}), \nabla \chi(\mathbf{X})). \quad (26)$$

The related limit problem then becomes

$$\Pi^{(0)}(\mathbf{x}^{(0)}) = \inf_{\chi \in \mathcal{V}^{(0)}} \Pi^{(0)}(\chi),$$

with

$$\Pi^{(0)}(\chi) = \int_B \bar{W}(\bar{I}_1(\chi), \bar{I}_2(\chi)) dV - W_{ext}(\mathbf{X}, \chi(\mathbf{X}), \nabla\chi(\mathbf{X})).$$

In this case, the space $\mathcal{V}^{(0)}$ incorporates the constraint $\det \mathbf{F} = 1$ in its construction. It is possible to show that a sequence of nearly-incompressible problems generated by $\varepsilon \rightarrow 0^+$ gives a subsequence of solutions $\{\mathbf{x}^\varepsilon\}$ that converges to $\mathbf{x}^{(0)}$ [5]. In other words, starting from a sequence of approximated incompressible problems, which have a demonstrated solution, it is then possible to obtain the solution of an incompressible problem according to a given precision.

3.2 Perturbed Lagrangian formulation

In practice, it is difficult and not necessary to construct a space $\mathcal{V}_h^{(0)}$ that satisfies exactly the incompressibility constraint $\det \mathbf{F} = 1$. It is not convenient also to utilize usual finite element spaces for $\mathcal{V}_h^\varepsilon$ when $\varepsilon \rightarrow 0^+$. It is more efficient to use a modified variational principle and the mixed finite element formulation.

The nearly-incompressibility form is obtained in terms of the saddle-point problem for (\mathbf{x}, p) , that is,

$$\Pi(\mathbf{x}, p) = \inf_{\chi \in \mathcal{V}} \sup_{q \in \mathcal{Q}} \Pi(\chi, q), \quad (27)$$

where

$$\begin{aligned} \Pi(\chi, q) &= \int_B [\bar{W}(\bar{I}_1(\chi), \bar{I}_2(\chi)) + q(J(\chi) - 1) \\ &\quad - G^*(q)] dV - W_{ext}(\mathbf{X}, \chi(\mathbf{X}), \nabla\chi(\mathbf{X})), \\ G^*(p) &= \sup_{J>0} \left[ph(J) - \frac{1}{\varepsilon} G(J) \right], \\ h(J(\mathbf{x})) &\equiv h(\nabla\mathbf{x}) = \det \mathbf{F} - 1 = J - 1 = 0. \end{aligned} \quad (28)$$

The variational form (27) is called perturbed Lagrangian formulation, because it relates to the traditional Lagrangian formulation through the addition of the term $-G^*(q)$ that relaxes the incompressibility condition.

Let (\mathbf{x}, p) be a stationary point of the functional Π . Then the variation $\delta\Pi$ is null, that is,

$$\int_B \left[\frac{\partial \bar{W}(\mathbf{x})}{\partial \bar{I}_1} \delta \bar{I}_1 + \frac{\partial \bar{W}(\mathbf{x})}{\partial \bar{I}_2} \delta \bar{I}_2 + p \delta J + (J(\mathbf{x}) - 1) \delta p - G^{*'}(p) \delta p \right] dV - \langle W'_{ext}(\mathbf{x}), \delta \mathbf{x} \rangle = 0.$$

As $\delta \mathbf{x}$ and δp are independent variations, the above equation can be rewritten as the following system of equations

$$\begin{aligned} \int_B \left[\frac{\partial \bar{W}(\mathbf{x})}{\partial \bar{I}_1} \delta \bar{I}_1 + \frac{\partial \bar{W}(\mathbf{x})}{\partial \bar{I}_2} \delta \bar{I}_2 + p \delta J \right] dV - \langle W'_{ext}(\mathbf{x}), \delta \mathbf{x} \rangle &= 0, \forall \delta \mathbf{x} \in \mathcal{V} \\ \int_B (J(\mathbf{x}) - 1) \delta p dV - \int_B G^{*'}(p) \delta p dV &= 0, \forall \delta p \in \mathcal{Q}. \end{aligned}$$

It is the starting point for the application of the mixed formulation to the problem.

From the assumed properties for $W(\bar{I}_1, \bar{I}_2, J)$, it follows that

$$\frac{\partial W}{\partial \bar{I}_1} \delta \bar{I}_1 + \frac{\partial W}{\partial \bar{I}_2} \delta \bar{I}_2 + \frac{\partial W}{\partial J} \delta J = \left(\frac{\partial W}{\partial \bar{I}_1} \frac{\partial \bar{I}_1}{\partial \mathbf{E}} + \frac{\partial W}{\partial \bar{I}_2} \frac{\partial \bar{I}_2}{\partial \mathbf{E}} + \frac{\partial W}{\partial J} \frac{\partial J}{\partial \mathbf{E}} \right) \cdot \delta \mathbf{E} = \mathbf{S} \cdot \delta \mathbf{E}.$$

Although $\frac{\partial W}{\partial J} = p$, it is more convenient from the numerical point of view to consider it as an independent variable. Therefore, (29)₁ is the equation obtained from the variational principle with the strain energy functional given in (20) and introducing the additional variable p . The constraint is represented variationally by equation (29)₂. It can be solved simultaneously to (29)₁ [33] or included in the problem using reduced selective integration [18] and projection methods [6].

3.3 Newton-Raphson Method for the Perturbed Lagrangian Formulation

For the saddle-point problem (27) defined in the time interval I_{n+1} , the solution can be obtained by solving a stationary point condition in terms of (29) rewritten below as

$$\begin{aligned} \delta \Pi(\mathbf{s}_{n+1}, \delta \mathbf{s}) &= D\Pi(\mathbf{s}_{n+1})[\delta \mathbf{s}] \\ &= \begin{cases} a(\mathbf{x}_{n+1}, \delta \mathbf{x}) + b_1(\delta \mathbf{x}, p_{n+1}) - l(\delta \mathbf{x}) = 0 \\ b_2(\mathbf{x}_{n+1}, \delta p) - g(p_{n+1}, \delta p) = 0 \end{cases}. \end{aligned} \quad (29)$$

with $\mathbf{x}_{n+1} \in \mathcal{X}_{n+1}, \forall \delta \mathbf{x} \in \mathcal{V}, p_{n+1}, \delta p \in \mathcal{Q}, \mathbf{s}_{n+1} = [\mathbf{x}_{n+1} \ p_{n+1}]^T, \delta \mathbf{s} = [\delta \mathbf{x} \ \delta p]^T$. The terms of the previous expression are

$$a(\mathbf{x}_{n+1}, \delta \mathbf{x}) = \int_{\mathcal{B}} \left[\frac{\partial \bar{W}(\mathbf{x}_{n+1})}{\partial \bar{I}_1} \delta \bar{I}_1 + \frac{\partial \bar{W}(\mathbf{x}_{n+1})}{\partial \bar{I}_2} \delta \bar{I}_2 \right] dV = \int_{\mathcal{B}} \bar{\mathbf{S}}_{n+1} \cdot \delta \mathbf{E} dV, \quad (30)$$

$$b_1(\delta \mathbf{x}, p_{n+1}) = \int_{\mathcal{B}} p_{n+1} \delta J dV, \quad (31)$$

$$b_2(\mathbf{x}_{n+1}, \delta p) = \int_{\mathcal{B}} (J(\mathbf{x}_{n+1}) - 1) \delta p dV, \quad (32)$$

$$g(p_{n+1}, \delta p) = \int_{\mathcal{B}} G^{*'}(p_{n+1}) \delta p dV. \quad (33)$$

The application of the Newton-Raphson method to (29) results in the following iterative procedure

$$\begin{aligned} \delta \Pi \left({}^{(k)}\mathbf{s}_{n+1}, \delta \mathbf{s} \right) + D\delta \Pi \left({}^{(k)}\mathbf{s}_{n+1}, \delta \mathbf{s} \right) \left[{}^{(k+1)}\Delta \mathbf{s} \right] &= 0, \\ {}^{(k+1)}\mathbf{s}_{n+1} &= {}^{(k)}\mathbf{s}_{n+1} + {}^{(k+1)}\Delta \mathbf{s}, \end{aligned} \quad (34)$$

and $k + 1 \rightarrow k$, until $\|{}^{(k+1)}\Delta \mathbf{s}\| \leq \varepsilon > 0$, observing that ${}^{(k+1)}\Delta \mathbf{s} = [{}^{(k+1)}\Delta \mathbf{u} \quad {}^{(k+1)}\Delta p]^T$ for the finite variation applied to ${}^{(k)}\mathbf{s}_{n+1}$.

The linearized term of (34) has the following general form

$$D\delta\Pi(\mathbf{s}, \delta\mathbf{s})[\Delta\mathbf{s}] = \begin{cases} D\delta W_{int}(\mathbf{s}, \delta\mathbf{s})[\Delta\mathbf{s}] - D\delta W_{ext}(\mathbf{s}, \delta\mathbf{s})[\Delta\mathbf{s}] \\ D\delta W_p(\mathbf{s}, \delta\mathbf{s})[\Delta\mathbf{s}] \end{cases} \quad (35)$$

Developing the first term of (35)

$$\begin{aligned} D\delta W_{int}(\mathbf{s}, \delta\mathbf{s})[\Delta\mathbf{s}] &= \int_{\mathcal{B}} \bar{\mathbf{C}}(\mathbf{x}) : D\mathbf{E}[\Delta\mathbf{u}] \cdot D\mathbf{E}[\delta\mathbf{x}] dV \\ &+ \int_{\mathcal{B}} \bar{\mathbf{S}} \cdot \left[\frac{1}{2} (\nabla\Delta\mathbf{u}^T \nabla\delta\mathbf{x} + \nabla\delta\mathbf{x}^T \nabla\Delta\mathbf{u}) \right] dV \\ &+ \int_{\mathcal{B}} \delta J Dp[\Delta p] dV + \int_{\mathcal{B}} p D\delta J[\Delta\mathbf{u}] dV. \end{aligned} \quad (36)$$

The stress terms and the tangent elasticity tensor are defined as

$$\mathbf{s} = \bar{\mathbf{S}} + \tilde{\mathbf{S}}, \quad (37)$$

$$\bar{\mathbf{C}}(\mathbf{x}) = \frac{\partial \bar{\mathbf{S}}}{\partial \mathbf{E}}(\mathbf{x}) = \frac{\partial^2 \bar{W}}{\partial \mathbf{E}^2}(\mathbf{x}), \quad (38)$$

where

$$\bar{\mathbf{S}} = \frac{\partial W}{\partial \bar{I}_1} \frac{\partial \bar{I}_1}{\partial \mathbf{E}} + \frac{\partial W}{\partial \bar{I}_2} \frac{\partial \bar{I}_2}{\partial \mathbf{E}}, \quad (39)$$

$$\tilde{\mathbf{S}} = p \frac{\partial J}{\partial \mathbf{E}}, \quad (40)$$

The expansion of the other terms in (36) results in

$$\delta J = \frac{\partial J}{\partial \mathbf{E}} \cdot D\mathbf{E}[\delta\mathbf{x}], \quad (41)$$

$$D\delta J[\Delta\mathbf{u}] = \frac{\partial J}{\partial \mathbf{E}} \cdot D\delta\mathbf{E}[\Delta\mathbf{u}] + D\mathbf{E}[\delta\mathbf{x}] \cdot D \left[\frac{\partial J}{\partial \mathbf{E}} \right] [\Delta\mathbf{u}], \quad (42)$$

$$\begin{aligned} p D\delta J[\Delta\mathbf{u}] &= p \frac{\partial J}{\partial \mathbf{E}} \cdot D\delta\mathbf{E}[\Delta\mathbf{u}] + D\mathbf{E}[\delta\mathbf{x}] \cdot p D \left[\frac{\partial J}{\partial \mathbf{E}} \right] [\Delta\mathbf{u}] \\ &= \tilde{\mathbf{S}} \cdot \left[\frac{1}{2} (\nabla\Delta\mathbf{u}^T \nabla\delta\mathbf{x} + \nabla\delta\mathbf{x}^T \nabla\Delta\mathbf{u}) \right] + \tilde{\mathbf{C}}(\mathbf{s}) : D\mathbf{E}[\Delta\mathbf{u}] \cdot D\mathbf{E}[\delta\mathbf{x}], \end{aligned} \quad (43)$$

and

$$\tilde{\mathbf{C}}(\mathbf{s}) = \frac{\partial \tilde{\mathbf{S}}}{\partial \mathbf{E}}(\mathbf{s}) = p \frac{\partial^2 J}{\partial \mathbf{E}^2}(\mathbf{x}). \quad (44)$$

Substituting (40) to (43) in (36), the term $D\delta W_{int}(\mathbf{s}, \delta\mathbf{s})[\Delta\mathbf{s}]$ can be rewritten in the following more convenient form

$$\begin{aligned} D\delta W_{int}(\mathbf{s}, \delta\mathbf{s})[\Delta\mathbf{s}] &= \int_{\mathcal{B}} \mathbf{C}(\mathbf{s}) : D\mathbf{E}[\Delta\mathbf{u}] \cdot D\mathbf{E}[\delta\mathbf{x}] \, dV \\ &+ \int_{\mathcal{B}} \mathbf{S} \cdot \left[\frac{1}{2} (\nabla\Delta\mathbf{u}^T \nabla\delta\mathbf{x} + \nabla\delta\mathbf{x}^T \nabla\Delta\mathbf{u}) \right] \, dV \\ &+ \int_{\mathcal{B}} D\mathbf{E}[\delta\mathbf{x}] \cdot \frac{\partial J}{\partial \mathbf{E}} Dp[\Delta p] \, dV, \end{aligned} \quad (45)$$

where $\mathbf{C} = \bar{\mathbf{C}} + \tilde{\mathbf{C}}$ and $\mathbf{S} = \bar{\mathbf{S}} + \tilde{\mathbf{S}}$.

Developing the second equation of (35), it follows that

$$\begin{aligned} D\delta W_p(\mathbf{s}, \delta\mathbf{s})[\Delta\mathbf{s}] &= \int_{\mathcal{B}} \delta p [DJ(\mathbf{x})[\Delta\mathbf{u}] - DG^{*'}(p)[\Delta p]] \, dV \\ &= \int_{\mathcal{B}} \delta p \left[D\mathbf{E}[\Delta\mathbf{u}] \cdot \frac{\partial J}{\partial \mathbf{E}} - DG^{*'}(p)[\Delta p] \right] \, dV. \end{aligned} \quad (46)$$

If the load is deformation independent, then $D\delta W_{ext}(\mathbf{s}, \delta\mathbf{s})[\Delta\mathbf{s}] = 0$ and the algorithm (34) assumes the form

$$\begin{aligned} \delta a \left({}^{(k)}\mathbf{s}_{n+1}; {}^{(k+1)}\Delta\mathbf{x}, \delta\mathbf{x} \right) + \delta b \left({}^{(k)}\mathbf{s}_{n+1}; \delta\mathbf{x}, {}^{(k+1)}\Delta p \right) &= l_{n+1}(\delta\mathbf{x}) - a \left({}^{(k)}\mathbf{x}_{n+1}, \delta\mathbf{x} \right) \\ &- b_1 \left(\delta\mathbf{x}, {}^{(k)}p_{n+1} \right) \end{aligned} \quad (47)$$

$$\begin{aligned} \delta b \left({}^{(k)}\mathbf{s}_{n+1}; {}^{(k+1)}\Delta\mathbf{x}, \delta p \right) &= \delta g \left({}^{(k)}p_{n+1}, {}^{(k+1)}\Delta p, \delta p \right) \\ &- b_2 \left({}^{(k)}\mathbf{x}_{n+1}, \delta p \right) + g \left({}^{(k)}p_{n+1}, \delta p \right) \end{aligned} \quad (48)$$

with ${}^{(k+1)}\mathbf{s}_{n+1} = {}^{(k)}\mathbf{s}_{n+1} + {}^{(k+1)}\Delta\mathbf{s}$; $k+1 \rightarrow k$ till $\|{}^{(k+1)}\Delta\mathbf{s}\| \leq \varepsilon > 0$. The terms of the previous expression are

$$\begin{aligned} \delta a \left({}^{(k)}\mathbf{s}_{n+1}; {}^{(k+1)}\Delta\mathbf{x}, \delta\mathbf{x} \right) &= \int_{\mathcal{B}} \mathbf{C} \left({}^{(k)}\mathbf{s}_{n+1} \right) : D\mathbf{E} \left[{}^{(k+1)}\Delta\mathbf{u} \right] \cdot D\mathbf{E}[\delta\mathbf{x}] \, dV \\ &+ \int_{\mathcal{B}} \mathbf{S} \left({}^{(k)}\mathbf{s}_{n+1} \right) \cdot \frac{1}{2} \left[\nabla {}^{(k+1)}\Delta\mathbf{u}^T \nabla\delta\mathbf{x} + \nabla\delta\mathbf{x}^T \nabla {}^{(k+1)}\Delta\mathbf{u} \right] \, dV, \\ \delta b \left({}^{(k)}\mathbf{s}_{n+1}; \delta\mathbf{x}, {}^{(k+1)}\Delta p \right) &= \int_{\mathcal{B}} D\mathbf{E}[\delta\mathbf{x}] \cdot \frac{\partial J}{\partial \mathbf{E}} \left({}^{(k+1)}\Delta p \right) \, dV, \\ \delta b \left({}^{(k)}\mathbf{s}_{n+1}; {}^{(k+1)}\Delta\mathbf{x}, \delta p \right) &= \int_{\mathcal{B}} \delta p \left\{ D\mathbf{E} \left[{}^{(k+1)}\Delta\mathbf{u} \right] \cdot \frac{\partial J}{\partial \mathbf{E}} \right\} \, dV, \\ \delta g \left({}^{(k)}p_{n+1}, {}^{(k+1)}\Delta p, \delta p \right) &= \int_{\mathcal{B}} \delta p \left\{ DG^{*'} \left({}^{(k)}p_{n+1} \right) \left[{}^{(k+1)}\Delta p \right] \right\} \, dV. \end{aligned}$$

3.4 Pressure projection method

The pressure projection method [6] is a generalization of the nearly-incompressible non linear hyperelastic B -bar model [18, 29] proposed for incompressible linear elasticity. Such techniques are called assumed deformation methods because they assume an interpolation for the deformation and tension fields independently of the adopted approximation for the displacement field. The hydrostatic pressure is projected in the least square sense on a previously chosen functional space and then rewritten in terms of displacements.

The projection technique consists in the problem of approximating a square integrable scalar function $p_e(\mathbf{x})$ in the domain of an element e in the least square sense through a linear combination of a sequence of functions $\mathbf{Q}(\mathbf{x}) = \{Q_1(\mathbf{x}), Q_2(\mathbf{x}), \dots, Q_n(\mathbf{x})\}$. It is necessary to determine the vector $\mathbf{p}_e = [p_1, p_2, \dots, p_n]^T$ that minimizes $\|p_e(\mathbf{x}) - \mathbf{Q}\mathbf{p}_e\|_{L_2(\mathcal{B}_e)}^2$, where $\|\cdot\|_{L_2(\mathcal{B}_e)}$ is the L_2 -norm in the element domain e .

The pressure projection method assumes the linear volumetric deformation/hydrostatic pressure hypothesis ($\tilde{\kappa}$ constant) which is reasonable in nearly-incompressible problems since the volumetric deformation is very small. Pressure projection corresponds to assuming a polynomial expansion for p inside the integration domain for the discrete problem. After that (29)₂ and (48)₂ are solved for the variable p as a function of the displacement. This result is then substituted in (29)₁ and (48)₁ in such a way that the resulting discrete system depends only on displacement.

The Babuska-Brezzi conditions supply the basis to choose the pressure and displacement functional spaces in a consistent way [4]. An usual choice is to utilize elements with Lagrange quadratic interpolation for the displacement field associated with the pressure linear expansion [6, 8, 33]. Numerical results have shown that constant interpolation inside the integration domain is satisfactory for hyperelasticity applications [9, 21]. For example, elements with serendipity quadratic displacement interpolation and constant pressure interpolation also respect the Babuska-Brezzi conditions. This choice facilitates the pressure condensation inside each element.

Applying (29)₂ to an integration domain $\mathcal{B}_e \subset \mathcal{B}$ with constant pressure \hat{p}_e , the following result is obtained

$$\int_{\mathcal{B}_e} (J - 1) \delta p \, dV - \int_{\mathcal{B}_e} G^{*'}(\hat{p}_e) \delta p \, dV = 0.$$

Therefore,

$$G^{*'}(\hat{p}_e) \int_{\mathcal{B}_e} dV = \int_{\mathcal{B}_e} (J - 1) \, dV.$$

In the case of a nearly-incompressible material, $G(J) = \frac{1}{2}(J - 1)^2$ is a reasonable choice for $G(J)$ [5, 21]. Therefore,

$$G^*(p) = \frac{1}{2}\varepsilon p^2 = \frac{1}{2\tilde{\kappa}}p^2 \Rightarrow G^{*'}(p) = \frac{p}{\tilde{\kappa}}.$$

Finally, the following expression is obtained

$${}^{(k)}\hat{p}_{e_{n+1}} = \frac{\tilde{\kappa}}{\int_{\mathcal{B}_e} dV} \int_{\mathcal{B}_e} \left[J \left({}^{(k)}\mathbf{x}_{n+1} \right) - 1 \right] dV. \quad (49)$$

It defines the hydrostatic pressure condensation in the domain \mathcal{B}_e . This expression can then be substituted in (48) and the variable ${}^{(k)}p_{n+1}$ is eliminated.

It can be seen in (49) that the projection method is a smoothing technique used to eliminate local oscillations of the pressure values. Therefore, it is coherent with the mixed formulation in which the pressure calculation is treated as a constraint to be respected in the mean sense.

Applying a similar procedure to the linearized system (48), it is possible to solve the second system of equation for the variable Δp , that is,

$$\int_{\mathcal{B}} DG^{*'}(p) [\Delta p] dV = \int_{\mathcal{B}} \left\{ D\mathbf{E}[\Delta \mathbf{u}] \cdot \frac{\partial J}{\partial \mathbf{E}} + J - 1 - G^{*'}(p) \right\} dV.$$

Assuming \hat{p}_e constant and using the previous expression for $G^*(p)$, then

$$\begin{aligned} {}^{(k+1)}\Delta \hat{p}_e &= \frac{\tilde{\kappa}}{\int_{\mathcal{B}_e} dV} \int_{\mathcal{B}_e} \left\{ D\mathbf{E} \left[{}^{(k+1)}\Delta \mathbf{u} \right] \cdot \frac{\partial J}{\partial \mathbf{E}} \left({}^{(k)}\mathbf{x}_{n+1} \right) \right. \\ &\quad \left. + J \left({}^{(k)}\mathbf{x}_{n+1} \right) - 1 - \frac{{}^{(k)}\hat{p}_{e_{n+1}}}{\tilde{\kappa}} \right\} dV, \end{aligned} \quad (50)$$

which is substituted in the first equation of the system.

4 Shape sensitivity analysis

4.1 Hyperelasticity without constraints

A family of structural problems may be defined by the association of the following variational problem to each domain \mathcal{B}_τ

$$a_{\mathcal{B}_\tau}(\mathbf{x}_\tau, \delta \mathbf{x}_\tau) = l_{\mathcal{B}_\tau}(\delta \mathbf{x}_\tau), \quad \forall \delta \mathbf{x}_\tau \in \mathcal{V}_\tau. \quad (51)$$

Consider a bilinear form given by

$$a_{\mathcal{B}_\tau}(\mathbf{x}_\tau, \delta \mathbf{x}_\tau) = \int_{\mathcal{B}_\tau} \mathbf{S}_\tau \cdot \delta \mathbf{E}_\tau dV = \int_{\mathcal{B}_\tau} \Theta_\tau (\nabla_\tau \mathbf{u}_\tau, \nabla_\tau \delta \mathbf{u}_\tau) dV. \quad (52)$$

Its total derivative with relation to the parameter τ is

$$[a_{\mathcal{B}_\tau}(\mathbf{x}_\tau, \delta \mathbf{x}_\tau)]' = \int_{\mathcal{B}} (\Theta'_\tau + \mathbf{V}_s \cdot \nabla_\tau \Theta_\tau + \Theta_\tau \operatorname{div} \mathbf{V}_s)_m (\det \mathbf{F}) dV. \quad (53)$$

For $\tau = 0$,

$$[a(x, \delta x)]' = \int_B (\Theta' + \mathbf{V} \cdot \nabla \Theta + \Theta \text{Div} \mathbf{V}) dV, \quad (54)$$

where

$$\Theta' = (\mathbf{S} \cdot \delta \mathbf{E})' = \mathbf{S}' \cdot \delta \mathbf{E} + \mathbf{S} \cdot \delta \mathbf{E}',$$

$$\nabla \Theta = \nabla (\mathbf{S} \cdot \delta \mathbf{E}) = \nabla \mathbf{S} \cdot \delta \mathbf{E} + \mathbf{S} \cdot \nabla \delta \mathbf{E}.$$

The terms in the previous equations are

$$\mathbf{S}' = \frac{\partial \mathbf{S}}{\partial \tau} = D_{\mathbf{E}} \mathbf{S} [\mathbf{E}'] = W_{,\mathbf{E},\mathbf{E}} : \mathbf{E}' = \mathbf{C}(x) : \mathbf{E}',$$

$$\mathbf{F}' = \frac{\partial \mathbf{F}}{\partial \tau} = \frac{\partial (\nabla \mathbf{x})}{\partial \tau} = \nabla \mathbf{x}' = \frac{\partial (\nabla \mathbf{u})}{\partial \tau} = \nabla \mathbf{u}',$$

$$\begin{aligned} \mathbf{E}' &= \frac{\partial \mathbf{E}}{\partial \tau} = \frac{1}{2} (\mathbf{F}'^T \mathbf{F} + \mathbf{F}^T \mathbf{F}') \\ &= D\mathbf{E} [\dot{\mathbf{u}}] + \mathbf{E}_{\mathbf{V}}(\mathbf{u}) - \frac{1}{2} [(\nabla \nabla \mathbf{u} \mathbf{V})^T \mathbf{F} + \mathbf{F}^T (\nabla \nabla \mathbf{u} \mathbf{V})], \end{aligned}$$

$$\mathbf{E}_{\mathbf{V}}(\mathbf{u}) = -\frac{1}{2} [(\nabla \mathbf{u} \nabla \mathbf{V})^T \mathbf{F} + \mathbf{F}^T (\nabla \mathbf{u} \nabla \mathbf{V})],$$

$$\begin{aligned} \delta \mathbf{E}' &= \frac{\partial \delta \mathbf{E}}{\partial \tau} = \frac{1}{2} (\delta \mathbf{F}^T \mathbf{F}' + \mathbf{F}^T \delta \mathbf{F}') + \frac{1}{2} (\delta \mathbf{F}^T \mathbf{F}' + \mathbf{F}^T \delta \mathbf{F}') \\ &= D\delta \mathbf{E} [\dot{\mathbf{u}}] + \delta \mathbf{E}_{\mathbf{V}}(\mathbf{u}) + \\ &\quad + \frac{1}{2} [(-\nabla \nabla \delta \mathbf{u} \mathbf{V})^T \mathbf{F} + \mathbf{F}^T (-\nabla \nabla \delta \mathbf{u} \mathbf{V})] \\ &\quad + \frac{1}{2} [\delta \mathbf{F}^T (-\nabla \nabla \mathbf{u} \mathbf{V}) + (-\nabla \nabla \mathbf{u} \mathbf{V})^T \delta \mathbf{F}], \end{aligned}$$

$$\begin{aligned} \delta \mathbf{E}_{\mathbf{V}}(\mathbf{u}) &= \frac{1}{2} [(-\nabla \delta \mathbf{u} \nabla \mathbf{V})^T \mathbf{F} + \mathbf{F}^T (-\nabla \delta \mathbf{u} \nabla \mathbf{V})] \\ &\quad + \frac{1}{2} [\delta \mathbf{F}^T (-\nabla \mathbf{u} \nabla \mathbf{V}) + (-\nabla \mathbf{u} \nabla \mathbf{V})^T \delta \mathbf{F}], \end{aligned}$$

$$\begin{aligned} \nabla \delta \mathbf{E} &= \frac{1}{2} [\nabla (\delta \mathbf{F}^T \mathbf{F} + \mathbf{F}^T \delta \mathbf{F})] \\ &= \frac{1}{2} [(\nabla \nabla \delta \mathbf{u})^T \mathbf{F} + \mathbf{F}^T (\nabla \nabla \delta \mathbf{u})] \\ &\quad + \frac{1}{2} [\delta \mathbf{F}^T (\nabla \nabla \mathbf{u}) + (\nabla \nabla \mathbf{u})^T \delta \mathbf{F}], \end{aligned}$$

$$\nabla \mathbf{S} = \mathbf{C}(\mathbf{x}) : \nabla \mathbf{E},$$

$$\nabla \mathbf{E} = \frac{1}{2} [\nabla (\mathbf{F}^T \mathbf{F})] = \frac{1}{2} [(\nabla \nabla \mathbf{u})^T \mathbf{F} + \mathbf{F}^T (\nabla \nabla \mathbf{u})].$$

Therefore,

$$\begin{aligned} [a(\mathbf{x}, \delta \mathbf{x})]' &= \int_{\mathcal{B}} \{ \mathbf{C}(\mathbf{x}) : D\mathbf{E}[\dot{\mathbf{u}}] \cdot \delta \mathbf{E} + \mathbf{S} \cdot D\delta \mathbf{E}[\dot{\mathbf{u}}] \} dV + \\ &+ \int_{\mathcal{B}} \{ \mathbf{C}(\mathbf{x}) : \mathbf{E}_{\mathbf{V}}(\mathbf{u}) \cdot \delta \mathbf{E} + \mathbf{S} \cdot \delta \mathbf{E}_{\mathbf{V}}(\mathbf{u}) + \mathbf{S} \cdot \delta \mathbf{E} \text{Div} \mathbf{V} \} dV. \end{aligned} \quad (55)$$

It is usual to rewrite (55) as the sum

$$[a(\mathbf{x}, \delta \mathbf{x})]' = \delta a(\mathbf{x}; \dot{\mathbf{u}}, \delta \mathbf{x}) + a'_V(\mathbf{x}, \delta \mathbf{x}), \quad (56)$$

where

$$a'_V(\mathbf{x}, \delta \mathbf{x}) = \int_{\mathcal{B}} \{ \mathbf{C}(\mathbf{x}) : \mathbf{E}_{\mathbf{V}}(\mathbf{u}) \cdot \delta \mathbf{E} + \mathbf{S} \cdot \delta \mathbf{E}_{\mathbf{V}}(\mathbf{u}) + \mathbf{S} \cdot \delta \mathbf{E} \text{Div} \mathbf{V} \} dV. \quad (57)$$

In the case of geometry independent loads, the sensitivity of $l(\delta \mathbf{x})$ with relation to the variation of \mathcal{B} is

$$\begin{aligned} \dot{l}(\delta \mathbf{x}) &= l'_V(\delta \mathbf{x}) \\ &= \int_{\mathcal{B}} [(\nabla \mathbf{b}_0) \mathbf{V} + \mathbf{b}_0 \text{Div} \mathbf{V}] \cdot \delta \mathbf{x} dV + \int_{\Gamma^2} [(\nabla \mathbf{t}) \mathbf{V} \mathbf{t} (\mathbf{V} \cdot \mathbf{n}) \text{Div} \mathbf{n}] \cdot \delta \mathbf{x} dA. \end{aligned} \quad (58)$$

Consequently, the sensitivity of the variational equation is given by

$$[a(\mathbf{x}_{n+1}, \delta \mathbf{x})]' = \dot{l}_{n+1}(\delta \mathbf{x})$$

or

$$\delta a(\mathbf{x}_{n+1}; \dot{\mathbf{u}}_{n+1}, \delta \mathbf{x}) + a'_V(\mathbf{x}_{n+1}, \delta \mathbf{x}) = \dot{l}'_{V_{n+1}}(\delta \mathbf{x}).$$

From these results, the variational equation for the direct method of shape sensitivity is [11]

$$\delta a(\mathbf{x}_{n+1}; \dot{\mathbf{u}}_{n+1}, \delta \mathbf{x}) = \dot{l}'_{V_{n+1}}(\delta \mathbf{x}) - a'_V(\mathbf{x}_{n+1}, \delta \mathbf{x}), \quad (59)$$

where $\delta a(\mathbf{x}_{n+1}; \cdot, \cdot)$ is the bilinear form of the last analysis iteration and \mathbf{x}_{n+1} is the solution of the response analysis in the iteration I_{n+1} .

The adjoint method for shape sensitivity is identical to the method developed for discrete parameter sensitivity, with the emphasis on the hypothesis of symmetric $\delta a(\mathbf{x}_{n+1}; \cdot, \cdot)$ [11]. Using

the adjoint equation, it is possible to eliminate the direct dependence with relation to $\dot{\mathbf{u}}_{n+1}$ and $\nabla \dot{\mathbf{u}}_{n+1}$ and the sensitivity expression of the functional ψ can be rewritten as

$$\begin{aligned} \dot{\psi} &= l'_{V_{n+1}}(\lambda) - a'_V(x_{n+1}, \lambda) + \int_{\mathcal{B}} [-\mathcal{G}_{,\mathbf{u}} \cdot \nabla \mathbf{u}_{n+1} \mathbf{V} - \mathcal{G}_{,\nabla \mathbf{u}} \cdot \nabla (\nabla \mathbf{u}_{n+1} \mathbf{V})] dV \\ &+ \int_{\mathcal{B}} [\mathcal{G} \text{Div} \mathbf{V} + \mathbf{V} \cdot \nabla \mathcal{G}] dV \end{aligned} \quad (60)$$

or

$$\dot{\psi} = l'_{V_{n+1}}(\lambda) - a'_V(x_{n+1}, \lambda) + \int_{\mathcal{B}} (\mathcal{G} \text{Div} \mathbf{V} - \mathcal{G}_{,\nabla \mathbf{u}} \cdot \nabla \mathbf{u}_{n+1} \nabla \mathbf{V}) dV. \quad (61)$$

4.2 Nearly-incompressible hyperelasticity

Consider now the following expressions

$$\begin{aligned} \mathbf{S}' &= \bar{\mathbf{S}}' + \tilde{\mathbf{S}}' = D_{\mathbf{E}} \bar{\mathbf{S}} [\mathbf{E}'] + D_{\mathbf{E}} \tilde{\mathbf{S}} [\mathbf{E}'] + D_p \tilde{\mathbf{S}} [p'] \\ &= \bar{W}_{,\mathbf{E},\mathbf{E}} : \mathbf{E}' + \tilde{W}_{,\mathbf{E},\mathbf{E}} : \mathbf{E}' + \tilde{W}_{,\mathbf{E},p} : p' \\ &= \bar{\mathbf{C}}(\mathbf{x}) : \mathbf{E}' + \tilde{\mathbf{C}}(s) : \mathbf{E}' + J_{,\mathbf{E}} p', \\ \dot{p} &= p' + \nabla p \cdot \mathbf{V} \Rightarrow p' = \dot{p} - \nabla p \cdot \mathbf{V}, \\ \nabla \mathbf{S} &= \mathbf{C}(\mathbf{x}) : \nabla \mathbf{E} + J_{,\mathbf{E}} \otimes \nabla p. \end{aligned}$$

The total derivative of the first equation in (29) in $\tau = 0$ is given by

$$\begin{aligned} [a(\mathbf{x}, \delta \mathbf{x}) + b_1(\delta \mathbf{x}, p)]' &= \int_{\mathcal{B}} [\mathbf{C}(s) : D\mathbf{E}[\dot{\mathbf{u}}] \cdot \delta \mathbf{E} + \mathbf{S} \cdot D\delta \mathbf{E}[\dot{\mathbf{u}}]] dV + \int_{\mathcal{B}} J_{,\mathbf{E}} \dot{p} \cdot \delta \mathbf{E} dV \\ &+ \int_{\mathcal{B}} [\mathbf{C}(s) : \mathbf{E}_{\mathbf{V}}(\mathbf{x}) \cdot \delta \mathbf{E} + \mathbf{S} \cdot \delta \mathbf{E}_{\mathbf{V}}(\mathbf{x}) + \mathbf{S} \cdot \delta \mathbf{E} \text{Div} \mathbf{V}] dV \\ &= \dot{l}(\delta \mathbf{x}) = l'_V(\delta \mathbf{x}), \end{aligned}$$

or

$$[a(\mathbf{x}, \delta \mathbf{x}) + b_1(\delta \mathbf{x}, p)]' = \delta a(\mathbf{s}; \dot{\mathbf{u}}, \delta \mathbf{x}) + \delta b(\mathbf{s}; \delta \mathbf{x}, \dot{p}) + a'_V(\mathbf{x}, \delta \mathbf{x}) + b'_{1V}(\delta \mathbf{x}, p) = l'_V(\delta \mathbf{x}),$$

For the second equation in (29), the result is

$$\begin{aligned} [b_2(\mathbf{x}, \delta p) - g(p, \delta p)]' &= \int_{\mathcal{B}_e} (J_{,\mathbf{E}} \cdot D\mathbf{E}[\dot{\mathbf{u}}] - DG^{*'}[\dot{p}]) \delta p dV \\ &+ \int_{\mathcal{B}_e} [J_{,\mathbf{E}} \cdot \mathbf{E}_{\mathbf{V}}(\mathbf{x}) + (J - 1 - G^{*'}) \text{Div} \mathbf{V}] \delta p dV = 0, \end{aligned}$$

or

$$[b_2(\mathbf{x}, \delta p) - g(p, \delta p)]' = \delta b(\mathbf{s}; \dot{\mathbf{u}}, \delta p) - \delta g(p, \dot{p}, \delta p) + b'_{2V}(\mathbf{x}, \delta p) - g'_V(p, \delta p). \quad (62)$$

The following system of equations in the unknowns $\dot{\mathbf{x}}_{n+1}$ and \dot{p}_{n+1} is obtained

$$\delta a(\mathbf{s}_{n+1}; \dot{\mathbf{u}}_{n+1}, \delta \mathbf{x}) + \delta b(\mathbf{s}_{n+1}; \delta \mathbf{x}, \dot{p}) = l'_{V_{n+1}}(\delta \mathbf{x}) - a'_V(\mathbf{x}_{n+1}, \delta \mathbf{x}) - b'_{1V}(\delta \mathbf{x}, p_{n+1}), \quad (63)$$

$$\delta b(\mathbf{s}_{n+1}; \dot{\mathbf{u}}_{n+1}, \delta p) = \delta g(p_{n+1}, \dot{p}_{n+1}, \delta p) - b'_{2V}(\mathbf{x}_{n+1}, \delta p) + g'_V(p_{n+1}, \delta p). \quad (64)$$

Applying the pressure projection method, it is possible to eliminate \dot{p} in the system (64) using the expression

$$\begin{aligned} \dot{p}_{n+1} &= \frac{\tilde{\kappa}}{\int_{\mathcal{B}_e} dV} \int_{\mathcal{B}_e} [J_{,\mathbf{E}} \cdot D\mathbf{E}[\dot{\mathbf{u}}_{n+1}] + J_{,\mathbf{E}} \cdot \mathbf{E}\mathbf{V}(\mathbf{x}_{n+1}) \\ &+ (J - 1 - G_{n+1}^*) \text{Div}\mathbf{V}] dV. \end{aligned} \quad (65)$$

In all the previous cases, the system response sensitivity until time t_{n+1} involves only unknowns of the time step t_{n+1} . It is independent of the equilibrium states of the previous time steps. In this way, the final system response sensitivity can be determined through a post-processing of the response analysis using only the equilibrium equation data of the last load step. The hyperelastic problem is reversible and the system response can be completely characterized by the initial and final states only.

5 Results

Engine suspension mounts are elements composed of rubber and metal, usually steel, designed to work as low and constant stiffness springs in the working range. These components are used as interfaces among subsets of mechanical systems to absorb vibrations. An example of application is the cushion of a vehicle power train (engine, clutch and gear). This set is fixed to the chassis of the vehicle by a suspension system composed of arms and cushions. It is possible to determine the cushion optimum positioning and the necessary stiffness from the natural frequencies and the vibration modes of each subsystem. The following step consists in adopting components that most approximate these stiffness characteristics or to design new cushions that fulfill the specifications in an optimum way.

A determined value of vertical stiffness is required for an engine mount application. Consider the cushion shown in Figure 1(a) and subjected to the load and boundary conditions of Figure 1(b). A plane deformation model is considered. The coefficients of the Mooney-Rivlin rubber material are $A_{10} = 0.138740 \text{ N/mm}^2$, $A_{01} = 0.05933 \text{ N/mm}^2$, $\tilde{\kappa} = 6599.2 \text{ N/mm}^2$; for the steel the linear isotropic properties are $E = 207 \times 10^3 \text{ N/mm}^2$ and $\nu = 0.3$. The geometry will be modified to fulfill suspension design specifications of the power train.

By making use of the two meshes shown in Figure 2, a vertical displacement of 9.0 mm was imposed on the upper face of the steel core in nine equal load steps. The force \times displacement plots are compared in Figure 3. It can be seen that the two meshes give practically identical

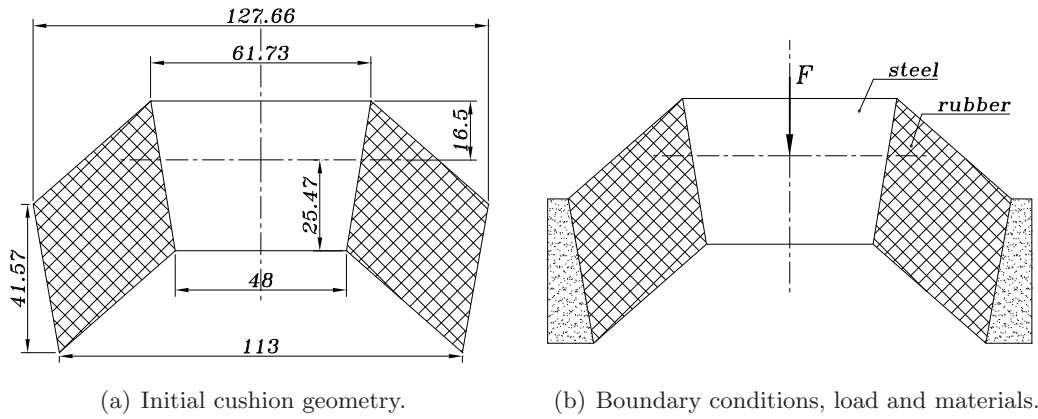
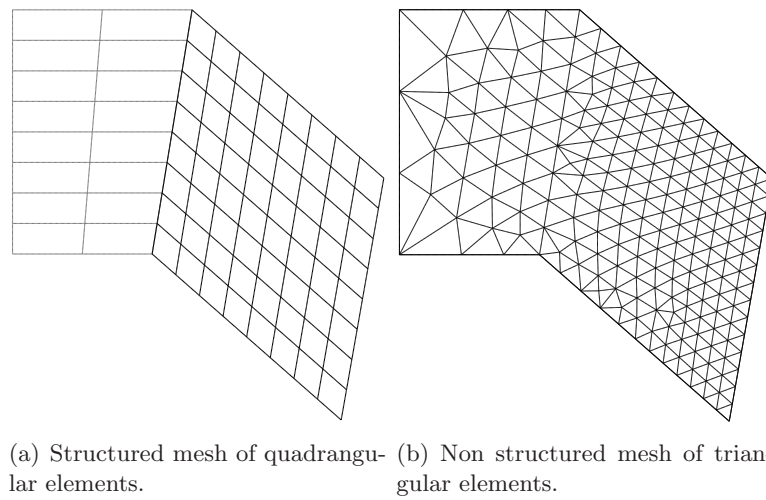


Figure 1: Cushion two dimensional model.

Figure 2: Mesh generation for the problem solution. Rubber volume of $1571.14802762 \text{ mm}^3$.

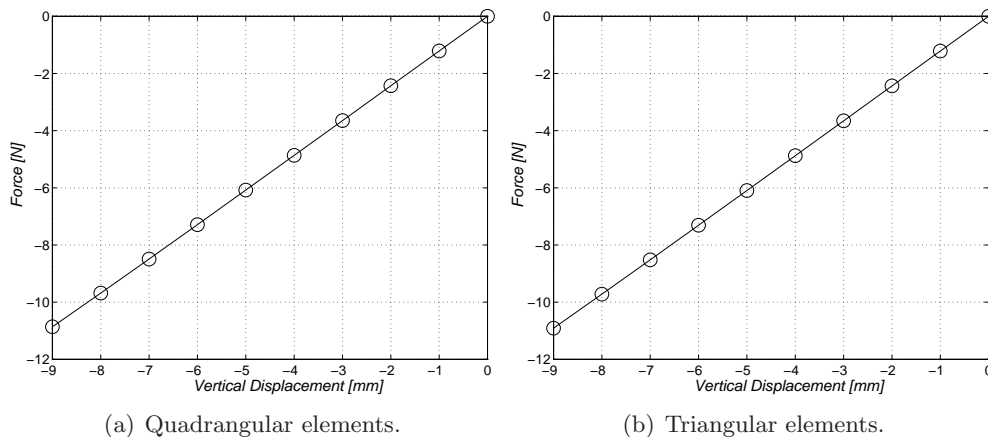


Figure 3: Force curves for vertical displacements with each mesh.

stiffness responses. According to these plots, the vertical stiffness of this component close to the displacement of -3.0 mm is 1.216 N/mm, while the application requires 0.810 N/mm. Therefore, the displacement of -3.0 mm must be attained for a force of -1.215 N in the symmetric model. The rubber volume can be decreased in order to reduce the cushion stiffness.

In terms of an optimization problem, the objective function is to minimize the rubber volume with the condition that the rubber core displacement be 3.0 mm for a vertical force of -1.215 N. The geometry parametrization is shown in Figure 4. The design variables are the coordinates x and y of the internal control points of two B-splines of degree 2 with 5 control points [28]. The initial values and the upper and lower bounds of each one of the 12 design variables are shown in Table 1. An additional restriction is that the strain energy does not exceed 2.5 Nmm. There are a total of 25 inequality restrictions, since each limit induces an inequality restriction in addition to the restriction in the strain energy and one equality restriction (steel core displacement).

The Herskovits interior point algorithm [16], the adjoint method of sensitivity, the mesh updating procedures and the velocity field with boundary fictitious displacements [27, 28] were used. Despite the quadrilateral structured mesh allows a more efficient solution, it could not be used because the first attempt to change the mesh (with the velocity fields and an external mesh generator) was rejected based on the mesh distortion criteria described in [28] for this element type. Consequently, the optimization algorithm could not continue the iterations. The problem solution with a non-structured triangular mesh is reached with 7 iterations and a total of 21 response analyses. The finite element mesh updating was based only on the repositioning of nodes using the velocity fields in all of the design modifications. It was not necessary to regenerate the mesh with an external generator. The evolution of the rubber volume in the sequence of iterations is shown in Figure 5(a). The value of the normalized displacement equality restriction is illustrated in Figure 5(b). This restriction is violated initially and satisfied within the required precision at the end of the optimization process.

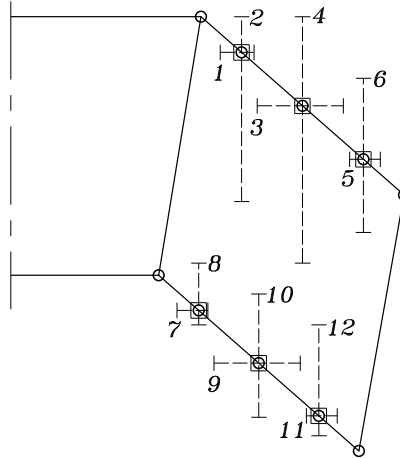
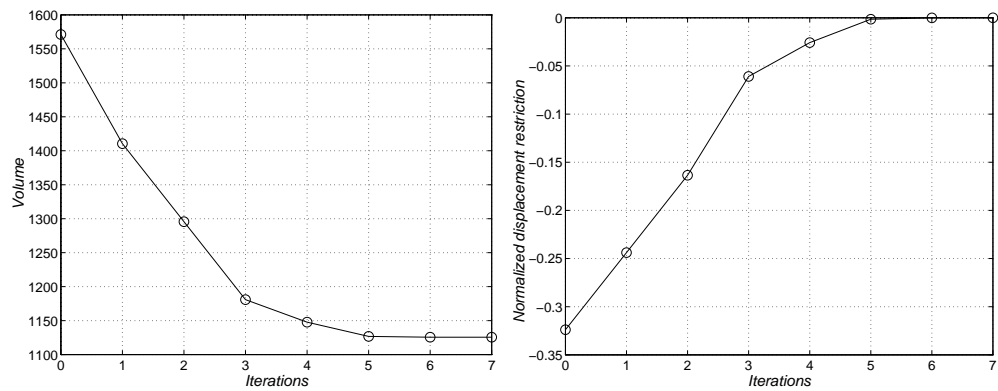


Figure 4: Design variables and respective bounds.

Table 1: Design variable values: initial, lower and upper bounds, optimum design [mm].

Variable	Initial	Lower	Upper	Optimum
1	117.4580	114.00	119.50	115.32006385
2	74.2140	50.00	80.00	67.74753867
3	127.3475	120.00	134.00	125.65323697
4	65.5350	40.00	80.00	56.16166904
5	137.2370	135.00	140.00	136.87073865
6	56.8560	45.00	70.00	49.10233489
7	110.5000	107.00	112.00	110.29317133
8	32.3240	30.00	40.00	38.72662048
9	120.2500	113.00	127.00	121.79908887
10	23.7650	15.00	35.00	32.65529169
11	130.0000	128.00	133.00	131.71769505
12	15.2060	12.00	30.00	21.15286329



(a) Objective function evolution (Rubber volume). (b) Evolution of the normalized displacement restriction.

Figure 5: Two dimensional model results.

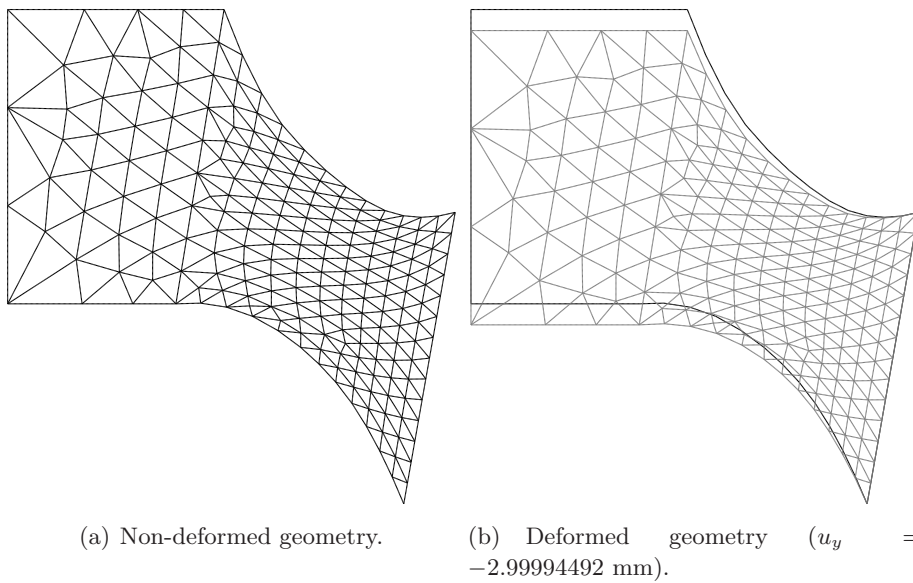


Figure 6: Optimal design. Rubber volume: $1125.55779686 \text{ mm}^3$. Strain energy: 1.84717475 Nmm .

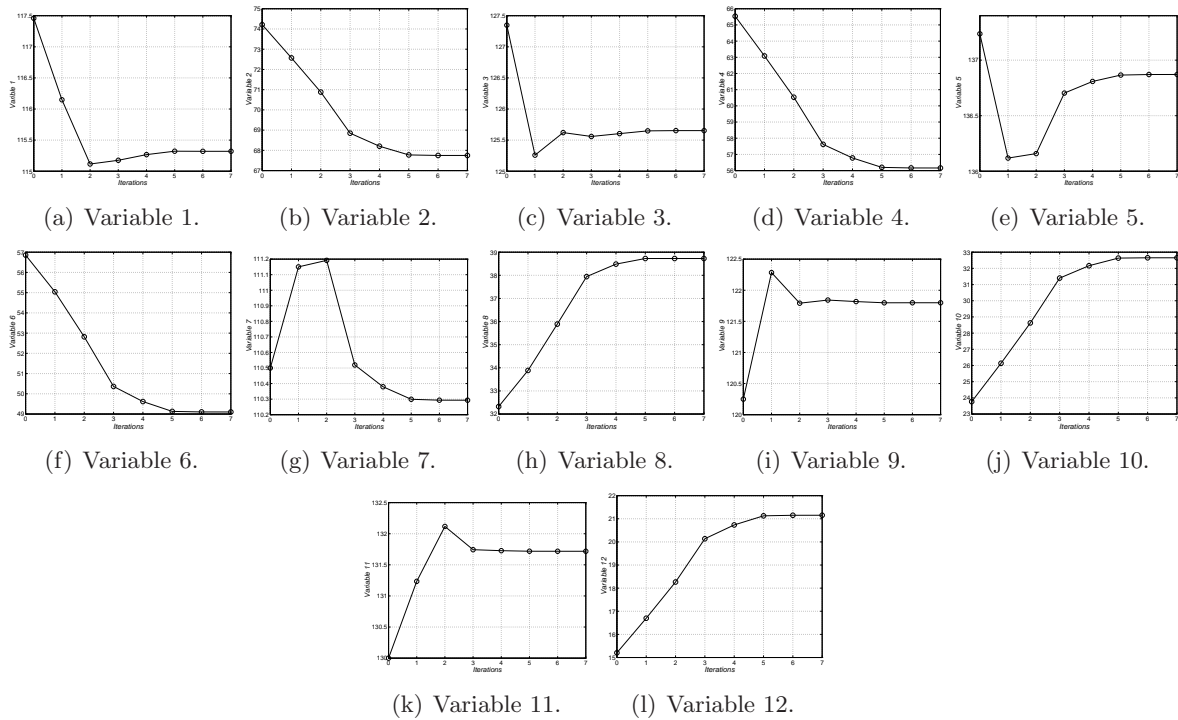


Figure 7: Historic of design variables [mm].

The mesh of the optimum design is shown in Figure 6. The final design is attained with a precision of 0.0001 for the convergence criterium of the minimization algorithm. At this iteration, the steel core vertical displacement is -2.99994492 mm and the rubber volume is 1079.00569837 mm³, which represents a reduction of 28.36% with relation to the original volume of 1571.14802762 mm³. The final mesh quality is quite reasonable. The historic of the design variables is shown in Figure 7.

A three dimensional cushion model is shown in Figure 8, where the boundary conditions are similar to the ones shown in Figure 1(b). Due to symmetry in directions x and z , only one quarter of the component was modeled. Making use of the two meshes shown in Figure 9, a vertical displacement of 1.0 mm was imposed on the upper face of the steel core in two equal load steps. The results show a stiffness of 40.684 N/mm in the neighborhood of this displacement. The application of this component requires a stiffness of 29.628 N/mm.

As in the 2D example, it is possible to formulate an optimization problem. The objective function is to minimize the rubber volume and simultaneously requires that the steel core displacement is 1.35 mm for a vertical force of -10.0 N for the symmetric finite element model (-40.0 N in the complete model). The geometry parametrization is shown in Figure 10. The design variables are the control point coordinates of the four NURBS surfaces. The initial values

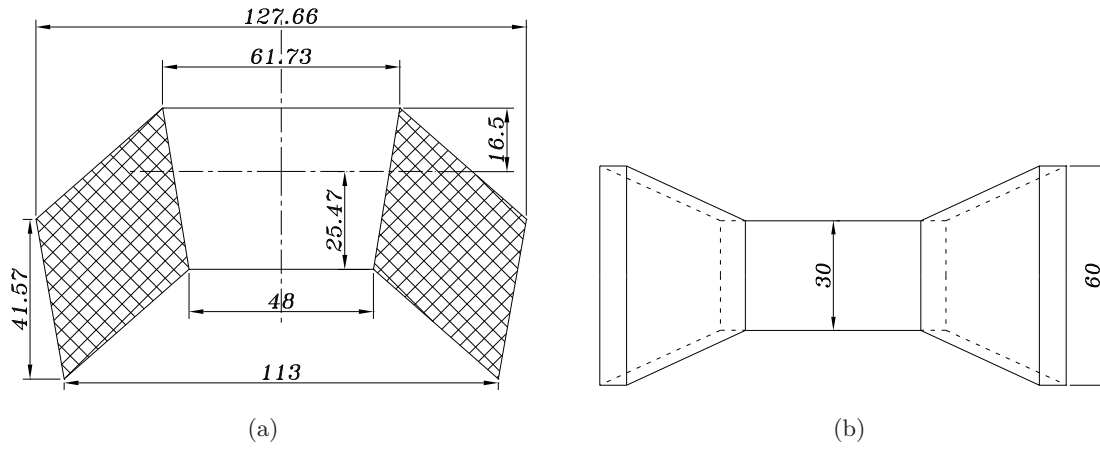


Figure 8: Cushion initial geometry.

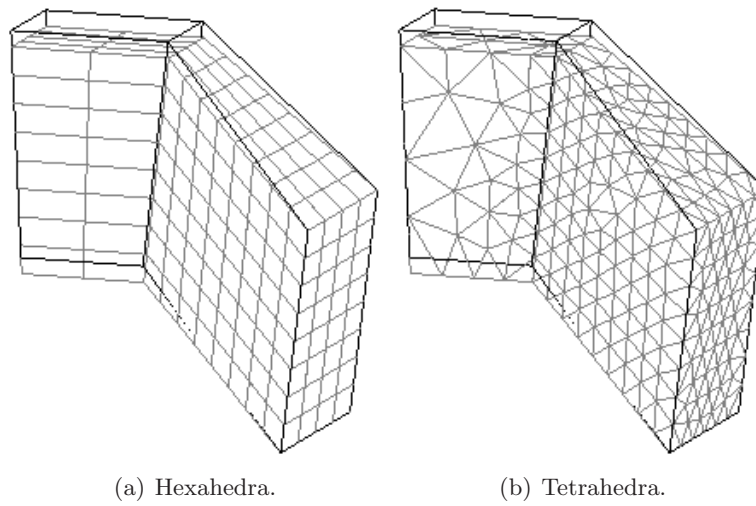


Figure 9: Deformed meshes of the initial geometry.

and the upper and lower bounds of each one of the 21 design variables are indicated in Table 2. An additional restriction is that the strain energy does not exceed 8.0 Nmm. There are 43 inequality restrictions and one equality restriction related to the steel core displacement. The mesh generation uses tetrahedral for more flexibility in the geometry modification during the optimization cycle.

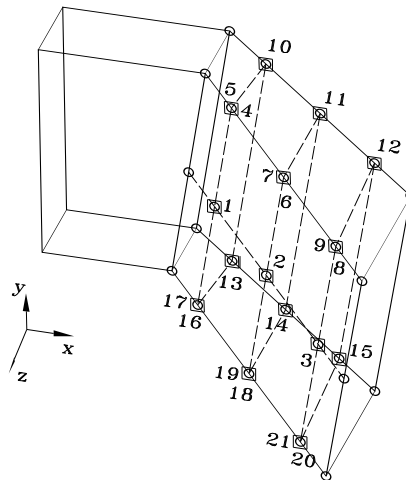


Figure 10: Design variables with respective limits.

The optimization problem is solved in 15 minimum iterations with precision of 0.0005 and 21 finite element analyses. The evolution of the rubber volume in the sequence of iterations is shown in Figure 11. Figure 12 illustrates the mesh of the optimum design. The vertical displacement of the steel core is -1.34999357 mm. The rubber volume is 28897.08171555 mm³ and represents a reduction of 18.26% compared to the original volume of 35351.15674344 mm³. It should be observed that the quality of the final mesh is quite reasonable.

6 Conclusions

This paper presented the shape optimization of 3D hyperelastic problems. The Mooney-Rivlin material model was used with the pressure project method. This method has an equivalent behavior when compared to the mixed formulation in terms of the pressure interpolation order. It also simplifies the implementation of incompressible material models in finite element codes based on displacements. The pressure constant and displacement quadratic interpolations were satisfactory for the nearly-incompressible material model. The elastomers of automotive cushions are relatively rigid and have moderate finite deformation. Therefore, the Mooney-Rivlin constitutive equation gives good results for such application. The use of meshes of triangles and tetrahedra with mesh updating and distortion control procedures were fundamental in the

Table 2: Design variables: meaning, initial values, upper and lower bounds, optimum value [mm].

Variable	Dir	Initial	Lower	Upper	Optimum
1	<i>z</i>	17.500000	14.0	18.5	14.01396844
2	<i>z</i>	22.500000	18.0	23.5	19.77219330
3	<i>z</i>	27.500000	23.5	28.5	23.51660888
4	<i>y</i>	55.891667	50.0	60.0	53.94129887
5	<i>z</i>	27.500000	23.5	28.5	23.52235259
6	<i>y</i>	65.535000	50.0	70.0	64.66501579
7	<i>z</i>	22.500000	20.0	24.5	24.45383121
8	<i>y</i>	75.178333	65.2	80.0	66.47478445
9	<i>z</i>	17.500000	15.0	18.5	16.57283684
10	<i>y</i>	74.214000	65.2	80.0	65.21299637
11	<i>y</i>	65.535000	50.0	70.0	61.87324420
12	<i>y</i>	56.856000	50.0	60.0	52.56456103
13	<i>y</i>	32.324000	28.0	35.0	34.84412684
14	<i>y</i>	23.765000	22.0	27.0	26.91077027
15	<i>y</i>	15.206000	14.0	18.5	18.47609098
16	<i>y</i>	14.255000	13.0	17.0	15.75345511
17	<i>z</i>	27.500000	23.5	28.5	23.52427786
18	<i>y</i>	23.765000	20.0	26.0	25.30741137
19	<i>z</i>	22.500000	18.0	23.5	18.39308939
20	<i>y</i>	33.275000	30.0	36.0	33.78082667
21	<i>z</i>	17.500000	14.0	18.5	14.95128675

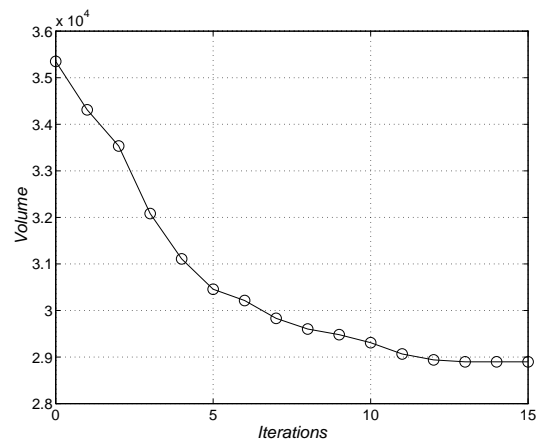


Figure 11: Objective function evolution (rubber volume).

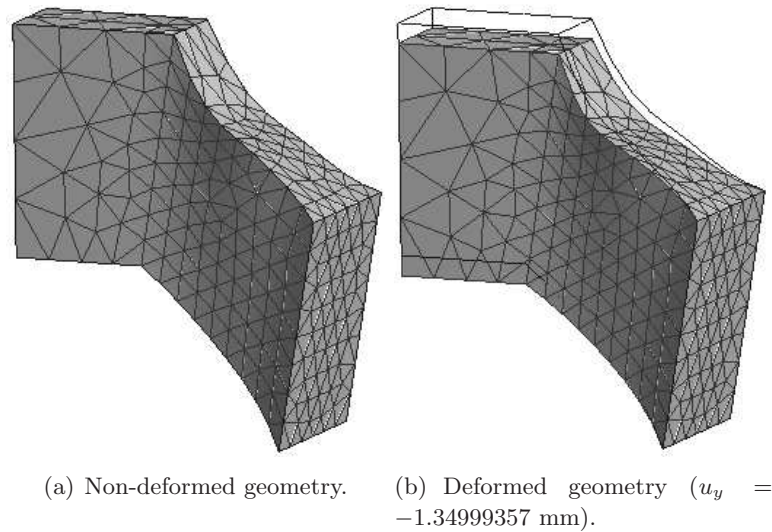


Figure 12: Optimum design. Rubber volume: 28897.08171555 mm³.

optimization cycle.

The behavior of the optimization procedure may be considered very good for the considered hyperelastic example. It is well known that large deformation hyperelasticity may present many difficulties for its numerical solution. For shape optimization of such problem, it is necessary to guarantee a controlled mesh distortion and geometry updating. These aspects were completely achieved for the example of a real 3D engineering problem.

References

- [1] D. Balagangadhar and D.A. Tortorelli. Design of large-deformation steady elastoplastic manufacturing processes. Part I: Displacement-based reference frame formulation. *International Journal for Numerical Methods in Engineering*, 49:899–932, 2000.
- [2] D. Balagangadhar and D.A. Tortorelli. Design of large-deformation steady elastoplastic manufacturing processes. Part II: Sensitivity analysis and optimization. *International Journal for Numerical Methods in Engineering*, 49:933–950, 2000.
- [3] J. Bonet and R.D. Wood. *Nonlinear Continuum Mechanics for Finite Element Analysis*. Cambridge University Press, Cambridge, 1997.
- [4] F. Brezzi and M. Fortin. *Mixed and Hybrid Finite Element Methods*. Springer Series in Computational Mathematics. Springer-Verlag, New York, 1991.
- [5] J.S. Chen, W. Han, C.T. Wu, and W. Duan. On the perturbed lagrangian formulation for nearly incompressible and incompressible hyperelasticity. *Computer Methods in Applied Mechanics and Engineering*, 142:335–351, 1997.

- [6] J.S. Chen and C. Pan. A pressure projection method for nearly incompressible rubber hyperelasticity, Part I: Theory. *Journal of Applied Mechanics*, 63:862–868, 1996.
- [7] J.S. Chen, C. Pan, and C.T. Wu. Large deformation analysis of rubber based on a reproducing kernel particle method. *Computational Mechanics*, 19:211–227, 1997.
- [8] J.S. Chen, C.T. Wu, and C. Pan. A pressure projection method for nearly incompressible rubber hyperelasticity, part II: Applications. *Journal of Applied Mechanics*, 63:869–876, 1996.
- [9] J.S. Chen, S. Yoon, H.P. Wang, and W. K. Liu. An improved reproducing kernel particle method for nearly incompressible finite elasticity. *Computer Methods in Applied Mechanics and Engineering*, 181:117–145, 2000.
- [10] K.K. Choi and W. Duan. Design sensitivity analysis and shape optimization of structural components with hyperelastic material. *Computer Methods in Applied Mechanics and Engineering*, 187(1-2):219–243, 2000.
- [11] K.K. Choi and N. Kim. *Structural sensitivity analysis and optimization*, volume 1 of *Mechanical Engineering Series*. Springer, New York, 2005.
- [12] G.P. Dias, J. Herskovits, and F.A. Rochinha. Simultaneous shape optimization and nonlinear analysis of elastic solids. In E. Oñate I. Idelsohn and E. Dvorkin, editors, *Computational Mechanics - New Trends and Applications*, pages 1–13, Barcelona, 1998. CIMNE.
- [13] L. Fourment and J.L. Chenot. Optimal design for non-steady-state metal forming processes - I: Shape optimization method. *International Journal for Numerical Methods in Engineering*, 39:33–50, 1996.
- [14] L. Fourment and J.L. Chenot. Optimal design for non-steady-state metal forming processes - II: Application of shape optimization in forging. *International Journal for Numerical Methods in Engineering*, 39:51–65, 1996.
- [15] I. Grindeanu, K.H. Chang, K.K. Choi, and J.S. Chen. Design sensitivity analysis of hyperelastic structures using a meshless method. *AIAA Journal*, 36(4):618–627, 1998.
- [16] J. Herskovits. A two-stage feasible directions algorithm for nonlinear constrained optimization. *Mathematical Programming*, 36:19–38, 1986.
- [17] J. Herskovits, A. Leontiev, G.P. Dias, and G. Santos. An interior point algorithm for optimal design of unilateral constrained mechanical systems. In E. Oñate I. Idelsohn and E. Dvorkin, editors, *Computational Mechanics - New Trends and Applications*, pages 1–17, Barcelona, 1998. CIMNE.
- [18] T. J. R. Hughes. Generalization of selective integration procedures to anisotropic and nonlinear media. *International Journal for Numerical Methods in Engineering*, 15:1413–1418, 1980.
- [19] G.W. Jang, Y.Y. Kim, and K.K. Choi. Remesh-free shape optimization using the wavelet-galerkin method. *International Journal of Solids and Structures*, 41(22-23):6465–6483, 2004.
- [20] G.W. Jang and Y.Y. Kimb. Sensitivity analysis for fixed-grid shape optimization by using oblique boundary curve approximation. *International Journal of Solids and Structures*, 42(11-12):3591–3609, 2005.
- [21] N. H. Kim. *Shape Design Sensitivity Analysis and Optimization of Nonlinear Static/Dynamic Structures with Contact/Impact*. PhD thesis, The University of Iowa, May 1999.

-
- [22] N.H. Kim and Y. Chang. Eulerian shape design sensitivity analysis and optimization with a fixed grid. *Computer Methods in Applied Mechanics and Engineering*, 194(30-33):3291–3314, 2005.
- [23] N.H. Kim, K.K. Choi, and J.S. Chen. Die shape design optimization of sheet metal stamping process using meshfree method. *International Journal for Numerical Methods in Engineering*, 51:1385–1405, 2001.
- [24] N.H. Kim, Y.H. Park, and K.K. Choi. Optimization of a hyper-elastic structure with multibody contact using continuum-based shape design sensitivity analysis. *Structural and Multidisciplinary Optimization*, 21(3):196–208, 2001.
- [25] A.M. Maniatty and M.F. Chen. Shape sensitivity analysis for steady metal-forming processes. *International Journal for Numerical Methods in Engineering*, 39:1199–1217, 1996.
- [26] R.W. Ogden. *Non-Linear Elastic Deformations*. Ellis Horwood Limited, Chichester, 1984.
- [27] C.A.C. Silva and M.L. Bittencourt. Effective integration of sensitivity analysis and minimization procedures with application to shape optimization of three-dimensional hyperelasticity. In *Proceedings of the 6th World Conference on Structural and Multidisciplinary Optimization*, <http://www.wcsmo6.org>, May 2005. University of Rio de Janeiro.
- [28] C.A.C. Silva and M.L. Bittencourt. Velocity fields using nurbs with distortion control for structural shape optimization. *Structural and Multidisciplinary Optimization*, 33(2):147–159, February 2007.
- [29] J.C. Simo and T.J.R. Hughes. *Computational Inelasticity*. Springer, New York, 1998.
- [30] D.E. Smith, D.A. Tortorelli, and C.L. Tucker. Analysis and sensitivity analysis for polymer injection and compression molding. *Computer Methods in Applied Mechanics and Engineering*, 167:325–344, 1998.
- [31] D.E. Smith, D.A. Tortorelli, and C.L. Tucker. Optimal design for polymer extrusion. Part I: Sensitivity analysis for nonlinear steady-state systems. *Computer Methods in Applied Mechanics and Engineering*, 167:283–302, 1998.
- [32] D.E. Smith, D.A. Tortorelli, and C.L. Tucker. Optimal design for polymer extrusion. Part II: Sensitivity analysis for weakly-coupled nonlinear steady-state systems. *Computer Methods in Applied Mechanics and Engineering*, 167:303–323, 1998.
- [33] T. Sussman and K.J. Bathe. A finite element formulation for nonlinear incompressible elastic and inelastic analysis. *Computers & Structures*, 26(1/2):357–409, 1987.
- [34] G. Zhao, E. Wright, and R. V. Grandhi. Preform die shape design in metal forming using an optimization method. *International Journal for Numerical Methods in Engineering*, 40:1213–1230, 1997.